Numerical Investigations of the Roles of Radiative and Evaporative Feedbacks in Stratocumulus Entrainment and Breakup

CHIN-HOH MOENG AND DON H. LENSCHOW

National Center for Atmospheric Research, Boulder, Colorado*

DAVID A. RANDALL

Colorado State University, Fort Collins, Colorado

(Manuscript received 11 May 1994, in final form 28 July 1994)

ABSTRACT

When the surface buoyancy flux is small and the shear is weak, turbulence circulations within a stratus-topped boundary layer are driven by two buoyancy-generating processes at cloud top: radiative cooling and evaporative cooling. These two processes respond very differently to entrainment, however. When the entrainment rate increases, the effectiveness of radiative cooling in driving circulations decreases (a negative feedback) but the effectiveness of evaporative cooling can increase (a positive feedback). The roles of these two competing feedbacks in determining the entrainment rate, and hence in determining cloud breakup, are examined in this paper through large eddy simulations.

Three stratus cases (with a small surface buoyancy flux) are simulated: one is stable with respect to the Lilly–Randall–Deardorff cloud-top entrainment instability criterion, and the other two are unstable. Only one of the two cloud decks in the unstable regime dissipates totally; the other remains nearly solid. A method is proposed to separate the cloud-top radiative and evaporative cooling contributions to downdraft acceleration, which drives the boundary-layer circulations. Analysis of these three flow fields shows that cloud dissipates totally only in the case that the evaporative feedback dominates. When the radiative feedback dominates, as in one of the unstable cases, the cloud remains nearly solid even though the Lilly–Randall–Deardorff criterion is satisfied.

To confirm the key role of cloud-top evaporative cooling in this positive feedback loop, two controlled experiments have been conducted—one with evaporative cooling turned off and the other with radiative cooling turned off—after the cloud was brought into the unstable regime with respect to the Lilly–Randall–Deardorff criterion. The cloud without evaporative cooling (for which boundary-layer circulations are driven only by cloud-top radiative cooling) remains solid, while that without radiative cooling (in which circulations are driven only by evaporative cooling) dissipates rapidly.

1. Introduction

The concept of cloud-top entrainment instability (CTEI), first applied to boundary-layer stratus clouds by Lilly (1968), is based on the following premise: If dry air parcels, entrained from the overlying inversion layer and then evaporatively cooled by mixing with cloudy air inside the cloud layer, become virtually colder than the cloudy air surrounding them, they can accelerate downward and penetrate deeply into the cloud layer. In this paper, we refer to the above mechanism as a necessary condition for CTEI and further restrict the definition of CTEI such that, as a result of the above process, the cloud layer dissipates totally.

This instability has been interpreted from two very different points of view. Some researchers have interpreted CTEI as a consequence of a small-scale mixing instability at cloud top due to buoyancy modification of mixtures of two different density fluids, one of which contains cloud droplets. This interpretation is derived from the above-mentioned necessary condition. Based on this interpretation, Lilly (1968) derived a CTEI criterion, which was further elaborated by Randall (1980) and Deardorff (1980b) to include water vapor and liquid water effects in the buoyancy of entrained parcels. However, the Lilly–Randall–Deardorff criterion (referred to hereafter as the LRD criterion) has been shown (by, e.g., Mahrt and Paumier 1982; Hanson 1984; Albrecht et al. 1985; Kuo and Schubert 1988; Albrecht 1991) to be in conflict with observations; persistent, solid stratiform cloud decks are often observed in the unstable regime. This led to the development of new CTEI criteria by, for example, MacVean and Ma-

* The National Center for Atmospheric Research is sponsored by the National Science Foundation.

Corresponding author address: Dr. Chin-Hoh Moeng, National Center for Atmospheric Research, P.O. Box 3000, Boulder, CO 80307-3000.

son (1990) based on energy conversion (from potential to kinetic energy) after entrainment mixing and by Siems et al. (1990) based on consideration of a range of mixtures, some of which are saturated and some of which are not (see Albrecht et al. 1985; Nicholls and Turton 1986). In Siems et al., the term "buoyancy reversal" is used to describe the above-mentioned necessary (but not sufficient) condition for CTEI. All these studies neglected the effects of turbulent dynamics within the boundary layer (i.e., boundary-layer circulations).

Others consider boundary-layer circulations to be a major player in CTEI (Albrecht et al. 1985; Boers 1991; Siems and Bretherton 1992; Moeng et al. 1992; Wang and Albrecht 1994; Krueger 1993). They interpret CTEI as follows: the inversion air that is entrained into the cloud layer is sufficiently dry that evaporative cooling, resulting from entrainment and subsequent mixing, becomes the dominant force in driving boundary-layer circulations. Under this condition, the following positive feedback (or instability) exists, coupling entrainment and boundary-layer circulations: As the entrainment rate increases, more dry air is brought into the cloud layer, the rate at which liquid water is evaporated increases, and so the intensity of evaporative cooling in the entrainment zone increases. As a result, the boundary-layer circulations are invigorated and they in turn increase the entrainment rate.

This kind of positive feedback does not occur, however, when we have longwave radiative cooling as the major driving force for boundary-layer circulations. As pointed out by Moeng and Schumann (1991) and Randall et al. (1992), the feedback loop between radiative cooling and entrainment (excluding evaporation) is negative. Entrainment brings warm air mostly into the downdraft branches of the circulations; this warm air (before evaporation occurs) mixes with radiatively cooled cloudy air and hence reduces the effectiveness of radiative cooling in driving boundary-layer circulations. Furthermore, increased entrainment reduces the liquid water mixing ratio near cloud top and so reduces the radiative cooling rate. Thus, without evaporative cooling, stronger entrainment reduces the effectiveness of longwave cooling in driving turbulent circulations within the boundary layer. In other words, the radiative feedback to entrainment rate is negative.

Of course, longwave radiation and evaporation are two different physical processes and they are not independent as we just described. Radiative cooling is a forcing process that can generate turbulent kinetic energy without any entrainment or mixing of two different air masses, as long as a cloud layer exists. On the other hand, evaporative cooling requires preexisting turbulent kinetic energy to incorporate air from above the PBL into the cloud layer and to mix them together. Nevertheless, both radiative and evaporative cooling at the cloud top can drive turbulence circulations in the same way; they both provide negative buoyancy in downdrafts near the cloud top and hence buoyantly drive boundary-layer turbulence. These cloud-top cooling processes are the dominant sources in the buoyancy flux equation when the surface heating is small.

We designed our large eddy simulations (LESs), described in section 2, to make the surface-heating contribution to driving the boundary-layer circulations negligible. As we have hypothesized above, the relative importance of radiative and evaporative cooling in driving boundary-layer circulations is likely to determine the sign of the feedback between entrainment and boundary-layer circulations and so determines whether or not cloud breakup occurs. In this paper, we focus on the difference in their responses to entrainment and show that the competition between the radiative feedback (which is negative) and the evaporative feedback (which can be positive) will determine the entrainment rate and, hence, cloud breakup. For this purpose, we split the cloud-top processes that drive (or damp) boundary-layer circulations into 1) cloud-top longwave radiative cooling, 2) cloud-top warming due to entrainment mixing (without evaporation), and 3) cloud-top evaporative cooling due to entrainment and mixing. The latter two processes result from entrainment of dry, warm inversion air: the second process, cloud-top warming due to entrainment mixing, is due only to the proportional buoyancy changes in the mixture density due to the combining of fluids of two densities, while the third process, cloud-top evaporative cooling, is the buoyancy change of mixture due to evaporation of cloud droplets in the mixture.

In LES, the major part of boundary-layer circulations and a significant part of the entrainment process are explicitly calculated, while longwave radiative and evaporative cooling are parameterized. Previous LES studies of CTEI have the following limitations: 1) restricting the turbulent field to two dimensions (Kuo and Schubert 1988; Siems et al. 1990; MacVean 1993), 2) resolving only one large eddy (Siems and Bretherton 1992), or 3) using a coarse grid resolution (Deardorff 1980a; Tag and Payne 1987). The turbulent PBL flow is inherently three-dimensional; the flow field simulated from a two-dimensional LES [e.g., Sykes and Henn's (1988) 2D simulation of Rayleigh–Bernard convective flow] looks laminar, rather than as chaotic as the 3D turbulent field in the PBL. Thus, we believe that only 3D simulations can generate realistic turbulent motions, for both shear- and buoyancy-driven PBL flows. Simulating one large eddy in a confined space could constrain the response of turbulent dynamics to CTEI. We use a numerical domain that allows for several large eddies to form simultaneously in each x or y direction. A significant portion of the entrainment process is due to the impinging of large updrafts onto the overlying inversion and consequently engulfing the inversion air back into the cloud layer. This occurs on scales of a few hundred meters in the horizontal and a few tens meters in the vertical (e.g., Mahrt and Paumier

1982; Caughey and Kitchen 1984; Breidenthal and Baker 1985). We will use a fine grid resolution that is at the upper limit of current computer capability, namely, 160 × 160 × 80 grid points in x, y, and z, such that the grid mesh is 12.5 m in all directions.

Cloud-top evaporation occurs when entrained air is sufficiently mixed with the cloudy air, so the rate at which the small-scale mixing process proceeds is crucial to determining the importance to the evaporation process. In LES, we assume that within each grid volume [i.e., $(12.5\ \text{m})^3$] complete mixing occurs as soon as air from above the PBL is entrained into cloudy air. Because of this assumption, and also because longwave radiative cooling is parameterized in LES, the simulated flow fields will be used only for a qualitative study of the CTEI mechanism, that is, to show the relative importance between the radiative and evaporative feedbacks, rather than in a quantitative search for a CTEI criterion or to test any of the previously proposed criteria. We attempt to be quantitative only when we compare among the three large eddy simulations.

2. Description of the large eddy simulations

Three LES stratus-topped PBLs, namely Stratus I, II, and III, were simulated using a grid mesh of 12.5 m in all three directions, a total domain size of 2 km × 2 km × 1 km, and a time step of 0.2 seconds. All simulations have a strong capping inversion at about 500 m, a constant geostrophic wind of 5 m s^{-1}, a large-scale divergence of $3 \times 10^{-6}\ s^{-1}$, and a constant sea surface temperature of about 284 K. The surface temperature is chosen to be about the same as the initial mixed-layer temperature (as given below) so that there is little heat flux from the surface. These three cases are designed such that all major buoyancy sources (or sinks) for driving boundary-layer circulations, that is, cloud-top longwave radiative cooling, cloud-top evaporative cooling, and entrainment-mixing warming, are near the cloud top. Detailed descriptions of the LES code can be found in Moeng (1986). It includes parameterized longwave radiative and latent heating processes that interact with the turbulence but excludes solar heating and drizzle.

The procedure used to generate these three different stratus cloud regimes is summarized in Fig. 1. (As described later in this section, and in section 4, two controlled experiments were run to confirm the role of cloud-top evaporation in cloud breakup.) The Stratus I experiment was initiated from a uniform laminar flow that has a constant wind u of 5 m s^{-1} everywhere in the domain. The initial liquid water static energy h_l/c_p, where c_p is the specific heat capacity, is about 285 K below 440 m, linearly increases to 297 K between 440 and 560 m, and linearly increases with a lapse rate of 6.5×10^{-3} K m^{-1} above 560 m. The initial total water mixing ratio q_T, which is specified to be 0.4 g kg^{-1} larger than the saturation mixing ratio at 440 m, is about

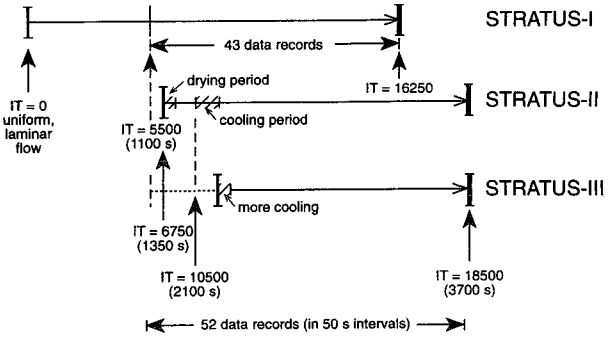

FIG. 1. A sketch showing the integration period for each of the simulations and the imposed drying and cooling periods. Numerical time steps are denoted as IT, and their associated simulation times (in s) are shown in parenthesis.

6.9 g kg^{-1} below 440 m, linearly decreases to 4 g kg^{-1} between 440 and 560 m, and remains at 4 g kg^{-1} above 560 m. Here, h_l is defined as $s_v - Lq_l$, where s_v is the virtual dry static energy, L the latent heat, and q_l the liquid water mixing ratio. For convenience, h_l and s_v are always scaled by c_p, so that they have units of K. After applying a small random perturbation at the first time step, the LES code was integrated for 16 250 steps, which is about 54 simulated minutes. The flow reaches a quasi-steady state during the last 30 min of the simulation. Starting from the 5500th time step, that is, ~18 min from the initial state, we stored 43 instantaneous flow fields at 50-s intervals on the National Center for Atmospheric Research (NCAR) Mass Storage System (MSS) for later analysis. Because of the strong inversion that was imposed, the PBL top remained at about 500 m. Stratus-I is stable with respect to the LRD criterion. Shen and Moeng (1993) showed that the large eddy structures in this simulation compare well with Nicholls' (1989) aircraft observations.

Stratus II was started from the 6750th time step of Stratus I, which is about 23 min of simulation from the initial laminar flow condition, and was subjected to the following two procedures. First, between the 6750th and 7000th time steps (i.e., for 50 simulated seconds), we *dried* the free-atmospheric air—above the *local* cloud tops—at a rate of 8×10^{-6} g kg^{-1} per time step; this is a first step to bring the cloud closer to the unstable regime with respect to the LRD criterion (see Fig. 3). This dried the above-cloud air a total of 2 g kg^{-1}. The simulation was then continued (without imposing further drying) for about 700 more seconds. Then, during the 10 500th–11 000th time step, we *cooled* the above-cloud air at a rate of 0.012 K per time step, for 100 s; this is a second step to bring the cloud into the unstable regime with respect to the LRD criterion (again, see Fig. 3). This gave a total of about 6 K cooling to the above-cloud air. The mean h_l and q_T, just before and after the imposed drying and cooling, are shown in Fig. 2a. The mean h_l became unstably

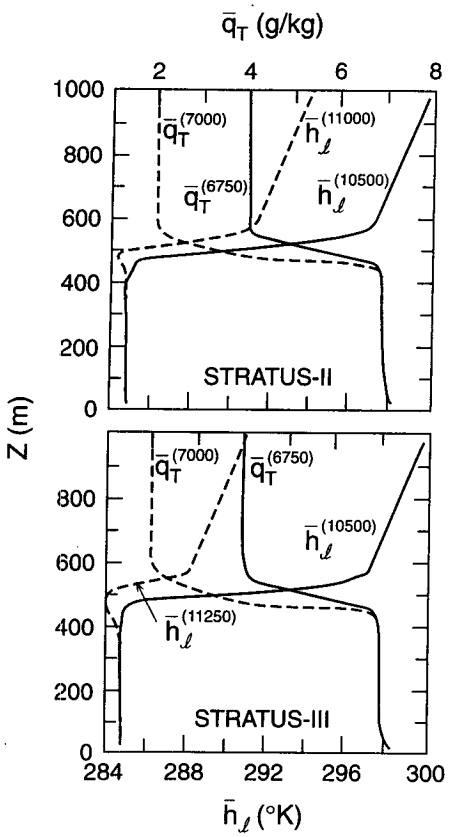

FIG. 2. Vertical distributions of the total water mixing ratio just before (solid curve) and after (dashed curve) the imposed drying and of the liquid water static energy just before (solid) and after (dashed) the imposed cooling in Stratus II and III.

stratified (decreasing with height) near cloud top because we cooled the inversion air above the *local* cloud tops, which includes air between the cloud-top domes. After the imposed drying and cooling, the free atmosphere becomes dry and cold enough to bring the cloud layer to the unstable regime with respect to the LRD criterion. The integration was continued (without imposing drying or cooling) for 1500 s, and data from the 5500th to 18.500th time step were stored at 50-s intervals on the NCAR MSS, for later analysis. As we will see, the cloud layer slowly started to break up for the first 12 min after the end of the cooling but then remained at about 85% fractional cloud cover during the last 12 min of the integration period.

To simulate a total breakup of a stratus cloud layer, we performed the same procedures in the Stratus III experiment as in Stratus II, except that we *cooled* the free-atmospheric air for a longer period of time, that is, from the 10 500th to 11 250th time step, which is a 150-s duration. This cooled the free-atmospheric air by a total of 9 K and brought the cloud layer further into the unstable regime with respect to the LRD criterion. Figure 2b shows the mean h_l and q_T, just before and after the imposed drying and cooling, for Stratus III. After the cooling procedure, the Stratus III simulation was continued for about 1500 s, and a total of 52 instantaneous flow fields were saved for analysis. As shown later, the cloud disappeared quickly and completely in this case.

The above drying and cooling changed the cloud-top jump condition, as shown in Fig. 3. Here, the cloud-top jumps $\Delta\theta_e$ and Δq_T are defined as the difference between the horizontal means of θ_e and q_T at levels z^+ and z^-, where z^+ is one grid level above the highest cloud-top domes and z^- is the LES level just below the lowest cloud-top level. (The equivalent potential temperature θ_e can be obtained from the simulated h_l field.) In Fig. 3, $\Delta\theta_e = 0$ is the Lilly's criterion, and the long dashed line shows the Randall–Deardorff criterion. The three diagonal straight lines represent $\Delta\theta_l = 0$ K, 5 K, and 10 K, respectively, where θ_l, the liquid water potential temperature, is a conserved thermodynamic variable (Betts 1973). The sharp decrease in the moisture jump between the 6750th and 7000th time step is due to the imposed drying, and the sharp decrease in the temperature jump between the 10 500th and 11 000th for Stratus II (and between the 10 500th and 11 250th time step for Stratus III) is due to the imposed cooling. Note that both Stratus II and Stratus III are well inside the unstable regime according to the LRD criterion even before they split at the 11 000th time step.

Our experimental design for simulating CTEI is not ideal. As we will see later, the imposed cooling of 6 K/100 s in Stratus II and 9 K/150 s in Stratus III

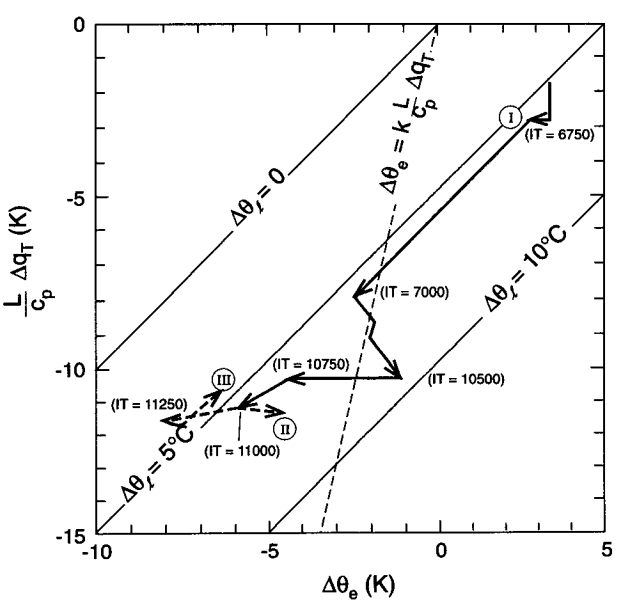

FIG. 3. A thermodynamic diagram showing time evolution of the cloud-top jump conditions during the simulations. The notations of I, II, and III in circles indicate the approximate positions of the jump conditions of Stratus I, II, and III, respectively, toward the end of each simulation.

drastically increases the layer-averaged turbulent kinetic energy within the PBL and, thus, greatly enhances the entrainment. This strong, artificially enhanced entrainment may have promoted the total break up of Stratus III before it had time to reach a quasi-steady state. Ideally, we would very gradually bring the cloud layer into the CTEI regime, but computational cost makes this approach infeasible at this time. [Each simulated minute took nearly 18 CRAY-YMP hours, of which 70% went for the longwave radiation calculation; the entire set of simulations reported here took more than two years to complete.] Nevertheless, for the current cases, it is interesting to compare Stratus II and III—both were abruptly brought into the unstable regime of LRD criterion—and to ask why cloud cover in the former case remains nearly solid, while in the latter it dissipates quickly.

Furthermore, to make sure that the strong, artificially enhanced entrainment due to our imposed cooling is not a major factor for the total breakup of Stratus III, we report on two controlled experiments, NO-EVP and NO-RAD, in section 4. These simulations are identical to Stratus III except that, after the 9 K/150 s free-atmospheric cooling, condensation–evaporation effects of the cloud are turned off in NO-EVP and radiation effects are turned off in NO-RAD.

3. Analyses and results

a. Time evolution of cloud-top height, cloud fraction, turbulent kinetic energy, and radiative cooling

Figures 4–6 show the time evolution of the horizontally averaged cloud-top height z_i, the fractional cloud cover σ_c, the layer-integrated (over the whole PBL) turbulent kinetic energy TKE, the horizontally averaged longwave radiative cooling rate at the level of its maximum Q_{rad}, and the liquid water mixing ratio at z_i, for Stratus I, II, and III, respectively. After the cloud begins to break, z_i is computed as the mean cloud-top height, averaged only over cloudy grid columns. The cloud cover is defined as the fraction of vertical grid columns that have liquid water. The abscissa is time in units of the record number (in 50-s intervals) stored in the NCAR MSS and in minutes of simulation.

Figure 4 shows that, throughout the Stratus I simulation, the cloud remains completely solid. The mean cloud-top height increases at the rate of about 6.5 $\times 10^{-3}$ m s^{-1} during the last 15 min. (The large-scale subsidence at z_i is about 1.4 $\times 10^{-3}$ m s^{-1}.) The turbulence has reached a quasi-steady state, so that, for example, the layer-averaged TKE does not fluctuate greatly after about 25 min from the initial laminar condition, that is, at about the eighth recorded flow field. The maximum horizontally averaged longwave radiative cooling rate is ~6–8 K h^{-1} throughout the simulation.

Figure 5a shows that, in Stratus II, cloud-top height increased steadily after the imposed cooling. The cloud

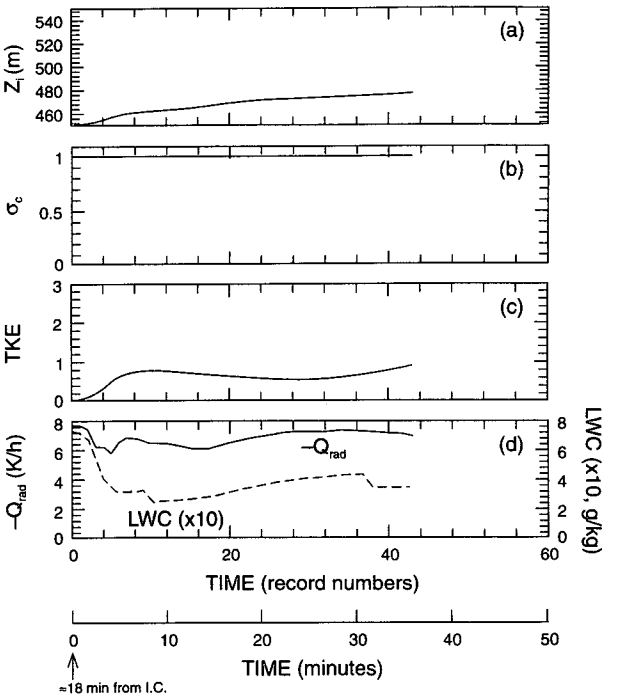

FIG. 4. Time evolution of (a) mean cloud-top height z_i, (b) fractional cloud cover, (c) vertically integrated turbulent kinetic energy, and (d) maximum horizontally averaged longwave radiative cooling, and the liquid water mixing ratio at z_i, for Stratus I.

started to break just after the imposed cooling but then remained at about 85% cloud cover after that, as shown in Fig. 5b. The layer-averaged TKE was modified very little by the imposed drying but was increased significantly by the cooling; shortly after the imposed cooling, the peak value of the TKE doubled due to local convective instability, resulting from the cooling of the air just above local cloud tops. After the TKE reached its maximum, it gradually decreased because of the gradual decrease in cloud-top longwave cooling (Fig. 5d) due to a decrease in cloud cover and in the cloud-top liquid water content, also shown in Fig. 5d. The cloud-top longwave cooling rate (horizontally averaged over both cloudy and clear regions) decreased to about 2 K h^{-1}, which is a factor of 3 smaller than that in Stratus I.

Figure 6 shows that the Stratus III mean cloud-top height grew quickly during and after the imposed cooling and remained nearly steady during the last 15 min of simulation. The fractional cloud cover decreased very rapidly, from 100% to 0% within the last 25 min of the simulation. About 2 min after the 9 K/150 s imposed cooling, the TKE level peaked at three times its previous value. The TKE then decreased sharply because of the large decrease in radiative cloud-top cooling (and evaporation, as shown later). When the cloud fraction became zero, there was no longer any cloud-top cooling for driving the turbulent kinetic energy and

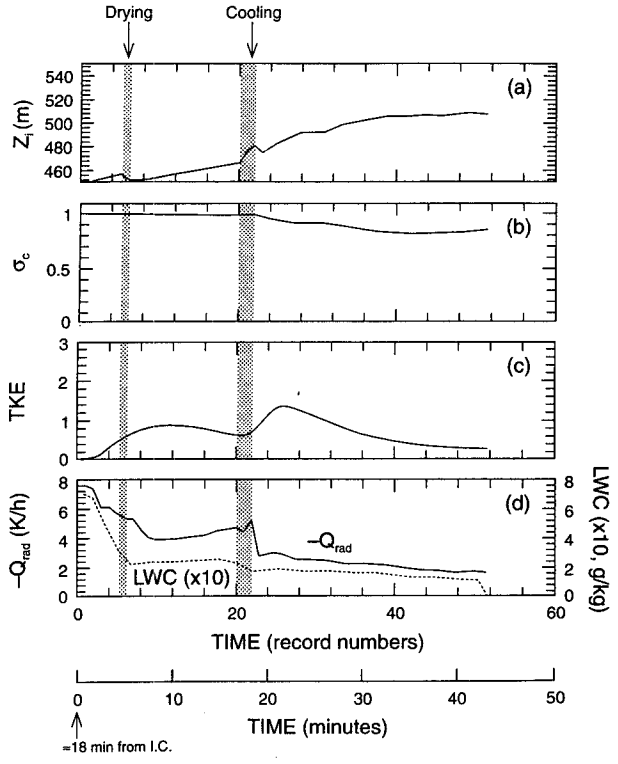

FIG. 5. Same as Fig. 4 but for Stratus II.

there was very little surface heating in this case. So, turbulence started to decay after that.

The positive feedback that we discussed in the introduction implies that the strength of the boundary-layer circulations (i.e., measured by the layer-averaged TKE) and entrainment rate should both increase with time, under idealized conditions when other factors (such as longwave radiative cooling) remain the same. In our Stratus II and III runs, cloud-top cooling (due to both radiation and evaporation) that drives the boundary-layer circulations decreased with time. Thus, we cannot use the time evolution of the TKE to study the feedback.

An indirect way to look at the feedback mechanism is to show that cloud-top evaporative cooling is indeed the major source in driving boundary-layer circulations in Stratus III but not in Stratus II. Then, according to the positive feedback mechanism described in the introduction, the cloud layer in Stratus III can break up totally. To do that, we need to separate the radiative and evaporative cooling effects on the buoyancy of downdrafts that drive boundary-layer circulations. We will discuss the method for separating these effects in section 3c.

To exclude the possibility that Stratus III broke up because the 9 K/150 s imposed cooling caused so much entrainment of dry air that the cloud simply dried out before it had a chance to reach a quasi-steady state, we will perform and analyze two controlled experiments, NO-EVP and NO-RAD, in section 4.

b. Cloud-top jump conditions

To show the time evolution of the jump conditions and to compare our results with previous theories, we calculated the criteria, using the same notation as Siems et al. (1993):

$$R = \frac{\overline{\theta}_e(z^+) - \overline{\theta}_e(z)}{\frac{L}{c_p}[\overline{q_T}(z^+) - \overline{q_T}(z)]} \sim \frac{\Delta\theta_e}{\frac{L}{c_p}\Delta q_T} \qquad (3.1)$$

(which was denoted by k in Kuo and Schubert 1988), where z is a layer just below the cloud top; R is the slope of the stability line in the $\Delta\theta_e - \Delta q_T$ diagram, as shown in Fig. 3. Thus, $R \sim 0.23$ shows the Deardorff–Randall criterion curve, and $R \sim 0.7$ shows the MacVean–Mason criterion curve (MacVean and Mason 1990). Our LES results, shown in (a) of Figs. 7–9, indicate that during the last 20 min of each simulation R is -0.8 in Stratus I, 0.4 in Stratus II, and 0.6 in Stratus III. Our cloud breakup R is much closer to MacVean and Mason's, although it still lies on their stable side.

We also examine the time evolution of the so-called buoyancy reversal, defined by Siems et al. (1990) as

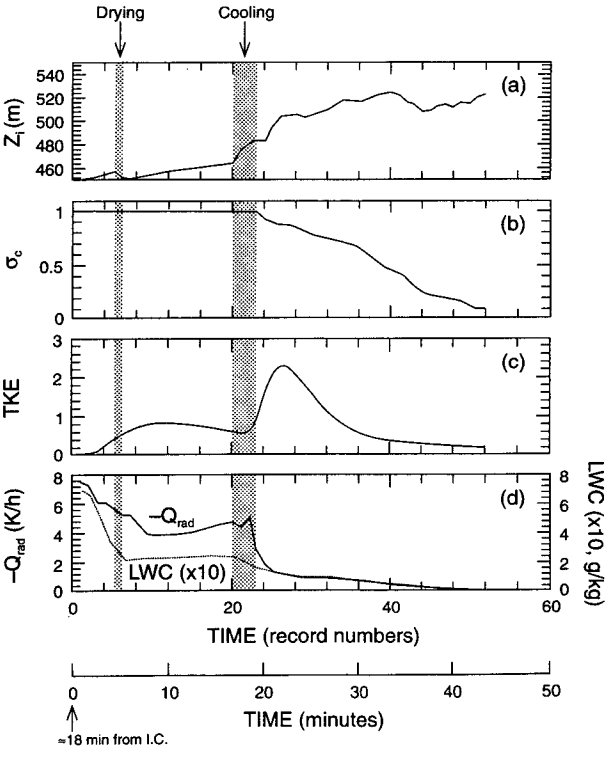

FIG. 6. Same as Fig. 4 but for Stratus III.

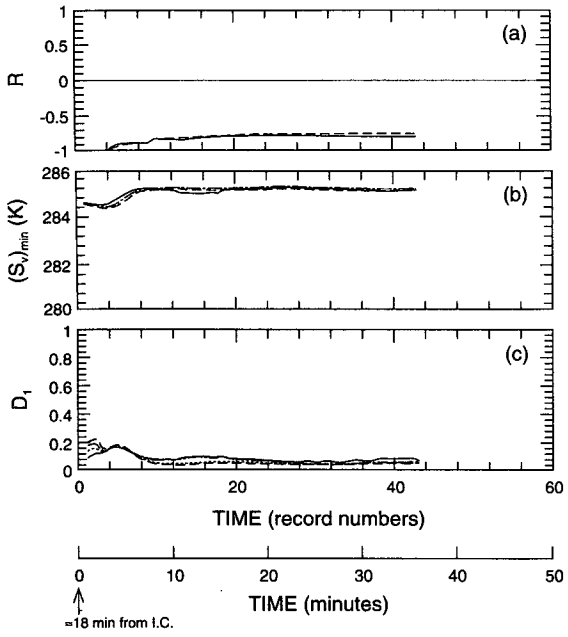

FIG. 7. Time evolution of (a) R value defined in (3.1), (b) minimum s_v on each x–y plane, and (c) D value defined in (3.2), where $(s_v)_{min}$ is taken from (b), for the four selected heights just below the cloud top for Stratus I.

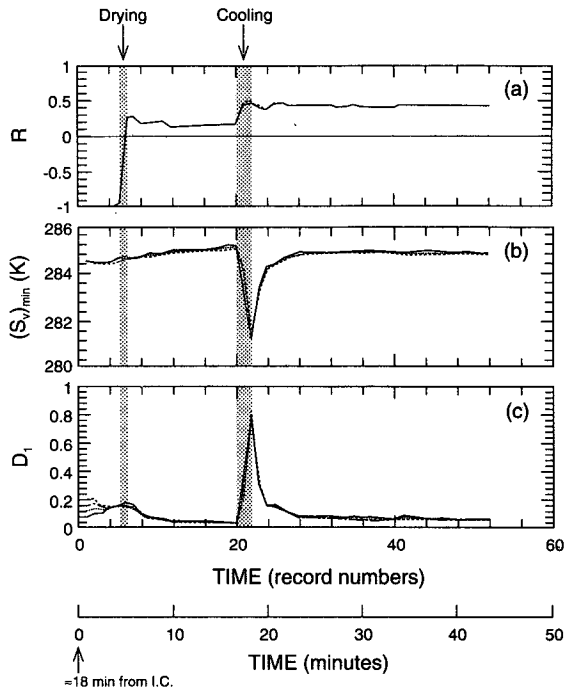

FIG. 8. Same as Fig. 7 but for Stratus II.

$$D = -\frac{(s_v)_{\min} - \overline{s_v}(z)}{\overline{s_v}(z^+) - \overline{s_v}(z)}, \qquad (3.2)$$

where z is at the lower fluid level, where its temperature is representative of that of the lower fluid before mixing with fluid from the z^+ layer. Using LES data, we can calculate the D value with two different methods. The first one, denoted here by D_1, is computed by choosing for use in (3.2) the minimum s_v on each LES horizontal plane at four representative heights close to the cloud top just below the interface, namely, z_1, z_2, z_3, and z_4. Here z_1 is one grid level below z_i, z_2 is two grid levels below z_i, and so on. For given $\overline{s_v}(z)$ and $\overline{s_v}(z^+)$, using the smallest possible $(s_v)_{min}$ yields the largest possible D value. Thus, D_1 is the upper limit on D. It is always positive, since $(s_v)_{min}$ is the minimum of all of the $s_v(x, y)$ that are averaged to make $\overline{s_v}(z)$. This value can be obtained from aircraft measurements by finding the minimum buoyancy just below the mean cloud-top height. A disadvantage of this approach is that this value includes effects not only from mixing and evaporative cooling but also from radiation, which is inherent in our LES flows and in field data. In addition, the levels just below cloud top in the LES flows or field data are far from uniform; they have turbulent motions in which updrafts are typically warmer than downdrafts. Thus, D_1 can be quite different from the D inferred by Siems et al. and others, who dealt with mixing of two uniform (laminar) fluid layers with no other active physical processes (such as radiation).

The value of $(s_v)_{min}$ and the implied D_1 value from our LES flow fields are shown in (b) and (c) of Figs. 7–9. Toward the end of each simulation, the minimum

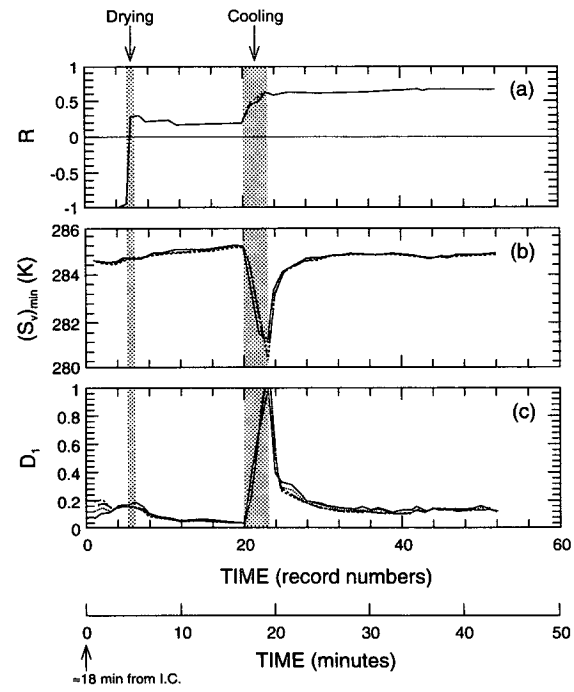

FIG. 9. Same as Fig. 7 but for Stratus III.

buoyancy approaches 285.2 K in Stratus I, 285 K in Stratus II, and 284.7 K in Stratus III, and all D_1 values become very small, that is, smaller than 0.2. The D_1 value in Stratus III is much smaller than the critical value of 1.3 obtained from laboratory experiments by Shy and Breidenthal (1990), except at the 23rd recorded flow time just after the imposed cooling, when $D_1 \sim 1$. We will show in section 4 that, with evaporative cooling turned off after the imposed cooling (the NO-EVP experiment), this large D_1 does not lead to a cloud breakup.

The second method of calculating D, described below and denoted here by D_2, is more directly related to the D discussed by Siems et al. because it is a measure of buoyancy reversal due *only* to mixing and evaporative cooling (see Nicholls and Turton 1986; Kuo and Schubert 1988). Here, we assume that our LES field consists of two constant density fluids, in which the upper one is clear air and the lower one is cloudy. Then after mixing, a minimum buoyancy occurs, due to evaporation, at a certain mixing fraction χ^*, at which the mixture is just saturated. Here, χ is the ratio of the free-atmospheric clear air to the cloudy air within the mixture. Of course, mixing fractions equal to χ^* may not actually occur in the LES results because physical processes other than evaporation and entrainment mixing also occur, and the LES flow is far from being a mixture of two constant density fluids. Nevertheless, χ^* can be derived as follows: buoyancy fluctuations (either θ_v' or s_v') can be expressed by the fluctuations of a conserved thermodynamic quantity (θ_e, θ_l, h, or h_l) and the total water mixing ratio q_T as

$$s_v' = A_1 h_l' + B_1 q_T' \quad \text{within clear air,} \tag{3.3}$$

and

$$s_v' = A_2 h_l' + B_2 q_T' \quad \text{within cloudy air,} \tag{3.4}$$

where the coefficients A_1, A_2, B_1, and B_2 vary according to the conservative thermodynamic variables chosen. Here, we use s_v and h_l as an example. The same coefficients are used in the definitions of Δ_1 and Δ_2 as follows:

$$\Delta_1 = A_1 \Delta h_1 + B_1 \Delta q_T \quad \text{for clear air,} \tag{3.5}$$

and

$$\Delta_2 = A_2 \Delta h_l + B_2 \Delta q_T \quad \text{for cloudy air.} \tag{3.6}$$

The Randall–Deardorff criteria (Randall 1980) is $\Delta_2 < 0$.

Note, Δ_1 and Δ_2 can be shown, using moist thermodynamics, to represent the slopes of the two curves in the buoyancy-mixing fraction diagram (e.g., Fig. 1 of Siems et al. 1990). The curve representing clear air (namely, $\chi > \chi^*$) has the slope

$$\left[\frac{\partial s_v(\chi)}{\partial \chi}\right] = \Delta_1; \tag{3.7}$$

while the slope for cloudy air (i.e., $\chi < \chi^*$) is

$$\left[\frac{\partial s_v(\chi)}{\partial \chi}\right] = \Delta_2. \tag{3.8}$$

Since the buoyancy at $\chi = \chi^*$, which is represented by $(s_v)_{\min}$ here and in (3.2) [although this buoyancy can be larger than the averaged $\overline{s_v}(z)$ in the stable regime with respect to the LRD criterion] as computed from the $\chi > \chi^*$ curve, has to agree with that computed from the $\chi < \chi^*$ curve, we have

$$(s_v)_{\min} = \overline{s_v}(z) + \chi^* \Delta_2 = \overline{s_v}(z^+) - (1 - \chi^*)\Delta_1, \tag{3.9}$$

where $\overline{s_v}(z)$ is at a level just below the mixing interface at z_i. This gives

$$\chi^* = \frac{\Delta_1 - \Delta\overline{s_v}}{\Delta_1 - \Delta_2}, \tag{3.10}$$

where $\Delta\overline{s_v} = \overline{s_v}(z^+) - \overline{s_v}(z)$. Using $(s_v)_{\min}$ defined in (3.9) in (3.2), D becomes

$$D_2 = -\frac{\chi^* \Delta_2}{\Delta\overline{s_v}}. \tag{3.11}$$

The D value so defined can be either negative or positive, depending on the sign of Δ_2.

The time evolutions of Δ_2, χ^*, $(s_v)_{\min}$, and D_2 are presented in Figs. 10–12; Δ_2 is about +2.0, −2.0, and −2.4 in Stratus I, II, and III, respectively. Note that Stratus II has a negative Δ_2, but its cloud deck remains nearly solid. The $(s_v)_{\min}$ calculated from (3.9), although slightly larger, is not very different from the actual minimum buoyancy shown in (b) of Figs. 7–9, except at the end of the imposed cooling period where the actual minimum buoyancy is much smaller. The mixing fraction χ^* is in the range of 0.16–0.2 in Stratus I, ~0.05 in Stratus II, and in Stratus III decreases from 0.08 during the imposed cooling period (i.e., 23rd recorded field) to nearly zero after the cloud cover becomes less than 20%. As a result, $D_2 \sim -0.05$ in Stratus I, ~0.02 in Stratus II, and in Stratus III decreases from ~0.04 during the imposed cooling period (23rd recorded field) to nearly zero after the cloud cover becomes less than 20%.

It is interesting to note that even though both D_1 and D_2 are derived from the same definition (3.2), they are very different in magnitude. Also, they have opposite signs in the stable regime with respect to the Randall–Deardorff criterion, that is, in Stratus I. In both Stratus II and III, D_2 is about one order of magnitude smaller than D_1, and also the large peak in D_1 just after the imposed cooling period does not show up in D_2.

Comparing Figs. 8 and 9, and also Figs. 11 and 12, we see no significant differences in these jump conditions between Stratus II and III. In other words, from these cloud-top jump conditions, which have been used in previous studies as criteria for CTEI, it is impossible to tell why one cloud deck dissipates totally and the

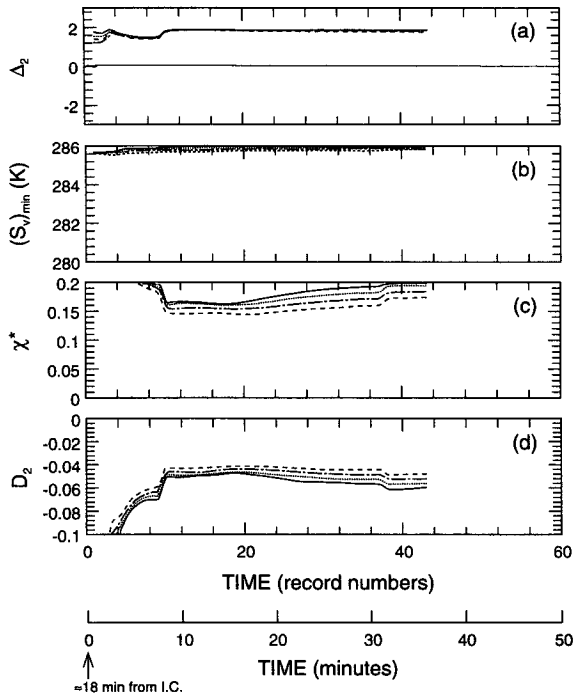

FIG. 10. Time evolution of (a) Δ_2 computed from (3.6), (b) $(s_v)_{min}$ from (3.9), (c) χ^* from (3.10), and (d) D value as defined in (3.11), for the four selected heights just below the cloud top for Stratus I.

other remains nearly solid. Therefore, in the following section, we examine the relative roles of the radiative and evaporative feedbacks in determining the fate of the cloud.

c. *Downdraft buoyancy due to longwave cooling, evaporative cooling, and entrainment-mixing warming*

As mentioned above, we need to separate the contributions of cloud-top radiative cooling from evaporative cooling in driving boundary-layer circulations to study the feedback mechanisms. Eddies that drive boundary-layer circulations within a stratus-topped boundary layer, when surface heating is small, are the near-cloud-top downdrafts, which emerge and accelerate downward from the entrainment zone. The air within these downdrafts can only come from two sources: neighboring updrafts through recirculating turbulent motions and the overlying free atmosphere through entrainment mixing, as shown in Fig. 13. The negative buoyancy of these downdrafts can then be enhanced locally by cloud-top longwave radiative and evaporative cooling, thus, promoting the boundary-layer circulations. Entrainment mixing (without evaporation) brings warm air into downdrafts, thus, damping the circulations. The relative contributions of these three physical processes (i.e., cloud-top radiative cooling, cloud-top evaporative cooling, and entrainment of warm inversion air into the cloud layer) in a stable, solid cloud layer have been studied in detail by Shao (1994), using one of our previously generated LES flow fields. They showed that for a particular LES stratus case, longwave radiation contributed −0.108 K, evaporation −0.027 K, and entrainment mixing 0.098 K to the buoyancy of near-cloud-top downdrafts (or more specifically, to the buoyancy fluctuations of downdrafts relative to the horizontal mean buoyancy in their analysis).

Here, we propose a more straightforward method to separate these cloud-top contributions. First, we define an effective mixing fraction f at each z just below the PBL top as

$$f(z) = \frac{\overline{q_T}^D(z) - \overline{q_T}^U(z)}{\overline{q_T}(z^+) - \overline{q_T}^U(z)}, \qquad (3.12)$$

where $\overline{q_T}^U$ and $\overline{q_T}^D$ are the total water mixing ratios averaged over all updrafts and all downdrafts, respectively, and z^+ is again the grid level just above the highest cloud domes, representing the overlying inversion air. Note that the mixing fraction computed from (3.12) is always larger than that computed from $[\overline{q_T}^D(z) - \overline{q_T}(z)]/[\overline{q_T}(z^+) - \overline{q_T}(z)]$ used by Shao (1994) or others, because on the average $\overline{q_T}^U$ is larger than $\overline{q_T}$, while $\overline{q_T}(z^+) - \overline{q_T}^U(z)$ is not too different from $\overline{q_T}(z^+) - \overline{q_T}(z)$.

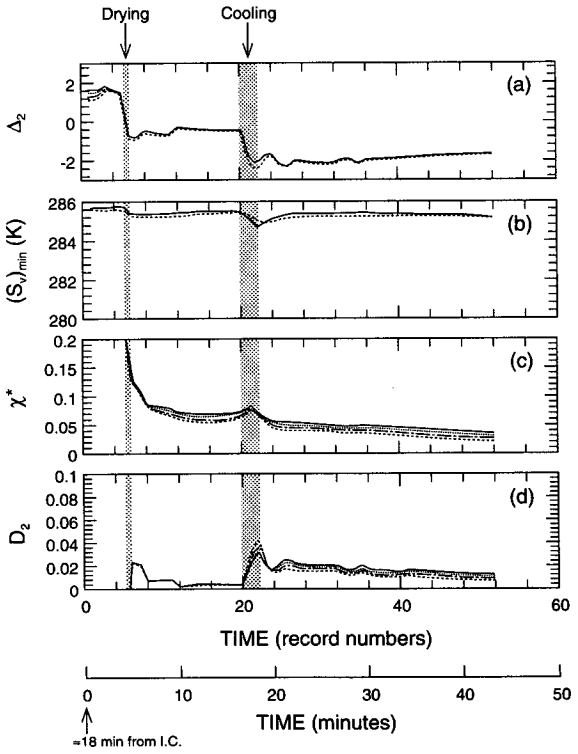

FIG. 11. Same as Fig. 10 but for Stratus II.

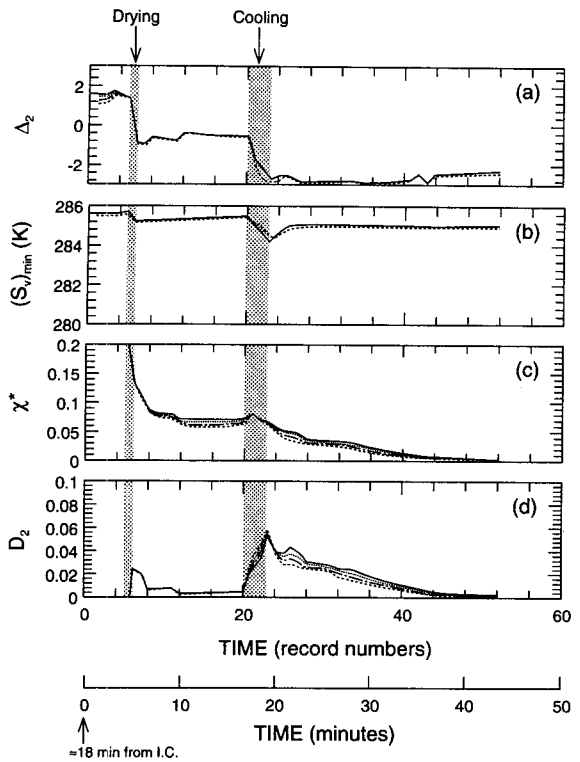

FIG. 12. Same as Fig. 10 but for Stratus III.

The physical meaning of f can be seen clearly if (3.12) is rewritten as

$$\overline{q_T}^D(z) = f\overline{q_T}(z^+) + (1-f)\overline{q_T}^U(z), \quad (3.13)$$

which means that f represents the portion of downdraft air that originated above the inversion, while the remaining downdraft air (i.e., $1-f$) comes from neighboring updrafts through recirculation as shown in Fig. 13. The total water mixing ratio within downdrafts cannot be modified by any other processes, such as radiation or evaporation. In nature it would be modified by drizzle. This effective mixing fraction concept was mentioned in Randall et al. (1992).

Equation (3.12) can also be rewritten as $\overline{q_T}^D(z) - \overline{q_T}^D(z) = f[\overline{q_T}(z^+) - \overline{q_T}^U(z)]$. This says that the difference of total water mixing ratio between updrafts and downdrafts resulting from entrainment mixing can be expressed as f times the mixing ratio difference between inversion air and updrafts. In reality, since the moisture supply from the surface is mostly in updrafts, the surface moisture flux can also affect the moisture difference between updrafts and downdrafts. We will apply our analysis only to the near-cloud-top levels, however, where the effects of the surface moisture flux can be neglected.

Using this effective mixing fraction, we estimated the relative contributions to the buoyancy of downdrafts due to cloud-top radiative cooling, evaporative cooling, and entrainment mixing (without evaporation) as follows. Similar to (3.13) but for the downdraft liquid water static energy $\overline{h_l}^D$, which can be modified by radiation as well as by mixing, we have

$$\overline{h_l}^D(z) = [f\overline{h_l}(z^+) + (1-f)\overline{h_l}^U(z)] + \Delta T_{rad}(z), \quad (3.14)$$

where ΔT_{rad} is a modification to the downdraft buoyancy (after mixing the inversion and updraft recirculating air) due solely to radiation (in our cases, due to longwave radiation only). Equation (3.14) gives

$$\Delta T_{rad}(z) = [\overline{h_l}^D(z) - \overline{h_l}^U(z)] - f(z)[\overline{h_l}(z^+) - \overline{h_l}^U(z)]. \quad (3.15)$$

Rewriting (3.15) as $\overline{h_l}^D(z) - \overline{h_l}^U(z) = f[\overline{h_l}(z^+) - \overline{h_l}^U(z)] + \Delta T_{rad}(z)$ shows that the h_l difference between updrafts and downdrafts can be due to both entrainment mixing ($f[\overline{h_l}(z^+) - \overline{h_l}^D(z)]$) and radiation ($\Delta T_{rad}$). Note that ΔT_{rad} is the amount of radiative cooling that contributes to the downdraft buoyancy fluctuations *relative to updrafts,* not *relative to the horizontal mean.*

Similar to (3.13) but for the virtual dry static energy, which can be modified by latent heating in addition to the above-mentioned two processes, we have

$$\overline{s_v}^D(z) = [f\overline{s_v}(z^+) + (1-f)\overline{s_v}^U(z)] + \Delta T_{rad}(z) + \Delta T_{evp}(z), \quad (3.16)$$

where ΔT_{evp} is the change of downdraft buoyancy due to latent heating, which includes evaporative cooling that resulted from entrainment mixing and latent heating that resulted from the air being cooled by radiation. Thus,

$$\Delta T_{evp}(z) = [\overline{s_v}^D(z) - \overline{s_v}^U(z)] - f[\overline{s_v}(z^+) - \overline{s_v}^U(z)] - \Delta T_{rad}(z). \quad (3.17)$$

Finally, we assume that the buoyancy difference between updrafts and downdrafts at levels close to the cloud top is due to entrainment mixing, evaporation,

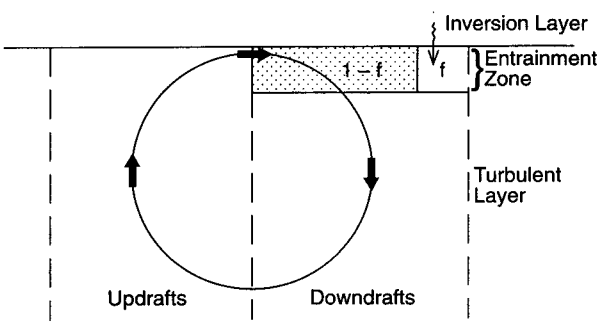

FIG. 13. A sketch showing the sources of air mass into downdrafts in the entrainment zone; f portion coming from the overlying inversion and $1-f$ from neighboring updrafts.

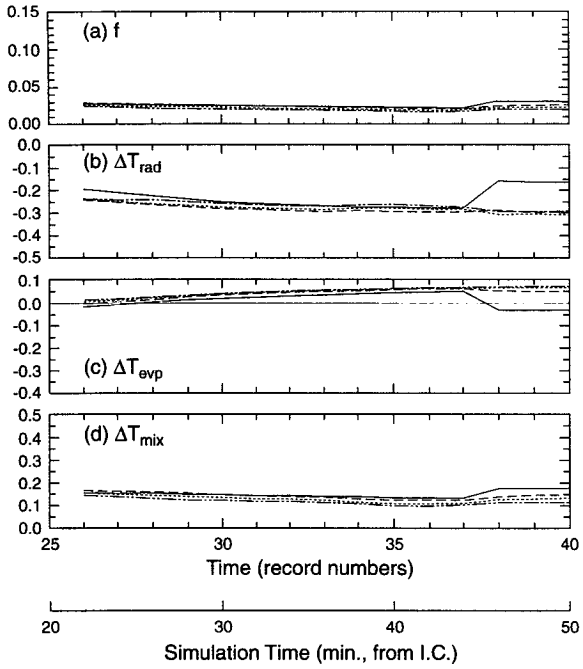

FIG. 14. Time evolution of (a) f computed from (3.12); the amounts of buoyancy changes of the near-cloud-top downdrafts due to (b) the longwave radiation, computed from (3.15); (c) condensation/evaporation, computed from (3.17); (d) entrainment mixing (without latent heat effect), computed from (3.19) for Stratus I. The four curves are for the four selected heights near the cloud top.

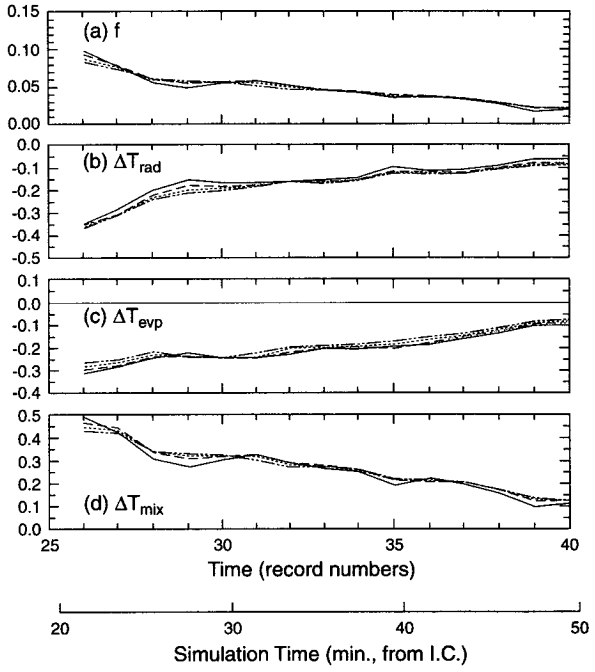

FIG. 15. Same as Fig. 14 but for Stratus II.

and radiation only. (Again, this means that we neglect the effects of the surface heat flux on the differences between updrafts and downdrafts at these near-cloud-top levels. Since surface heat flux is small in the present case, this is not a serious problem.) In this way, we obtain

$$\overline{s_v}^D(z) - \overline{s_v}^U(z) = \Delta T_{\text{mix}}(z) + \Delta T_{\text{rad}}(z) + \Delta T_{\text{evp}}(z), \tag{3.18}$$

where ΔT_{mix} is the buoyancy change of downdrafts due to incorporating a fraction f of inversion air into the recirculating air mass from neighboring updrafts. Comparing (3.17) with (3.18), we then have

$$\Delta T_{\text{mix}}(z) = f[\overline{s_v}(z^+) - \overline{s_v}^U(z)]. \tag{3.19}$$

In the following, we will use (3.12) to calculate the mixing fraction f, (3.15) for ΔT_{rad}, (3.17) for ΔT_{evp} and (3.19) for ΔT_{mix}, at four levels very close to the cloud top; that is, levels z_1, z_2, z_3, and z_4 defined in section 3b. Schumann and Moeng (1991) and Moeng et al. (1992) have shown that the thermodynamic differences between updrafts and downdrafts are closely related to the heat flux. Thus, according to (3.18) ΔT_{rad}, ΔT_{evp}, and ΔT_{mix} also represent the contributions of these three physical processes to the near-cloud-top buoyancy flux. The results are shown in Figs. 14–16, for the three simulations. Only 15 LES fields from the 26th (about 2 min after the imposed cooling) to 40th recorded LES datasets (before the Stratus III broke up totally) are shown here. (Before the 26th recorded field, just after the cooling procedure that results

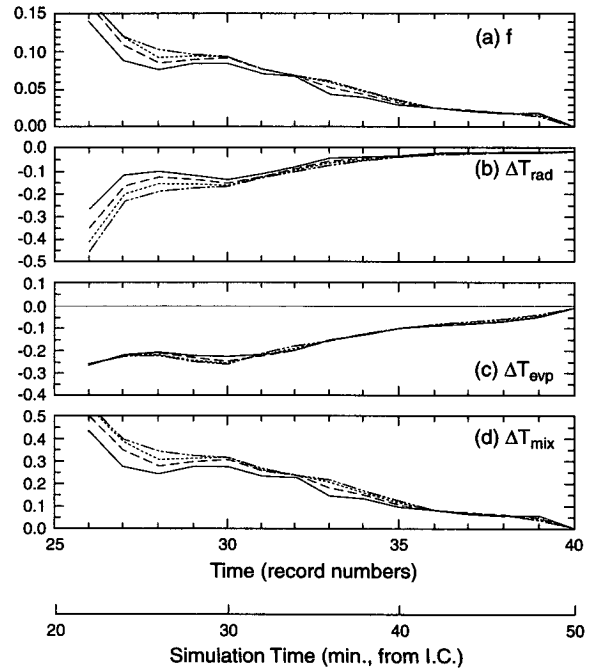

FIG. 16. Same as Fig. 14 but for Stratus III.

in strong entrainment, the mixing fraction and all of these ΔT contributions are too large to plot on the scales used in Figs. 14–16.) During this time period, the layer cloud amounts at these four levels, respectively, (which are slightly different from the total cloud amounts σ_c shown in Figs. 4b–6b) are constant at 100% in Stratus I, stay constant at about 75% in Stratus II, and decrease from 60% to about 20% in Stratus III. First, we see that there is little difference in results for the four selected heights. The buoyancy changes for each process we show here are quite different from, but overall about twice as large as, previous estimates (e.g., Nicholls 1989; Wang and Albrecht 1994; and Shao 1994). This is because (a) the method we used here in defining the mixing fraction f is quite different; (b) these are different cases; and (c) our ΔT contributions are to the buoyancy fluctuations of downdrafts *relative to updrafts* [i.e., (3.18)], not *relative to the horizontal mean.* This alone could result in a doubling of ΔT. (See Figs. 5 and 6 in Moeng et al. 1992.)

Figure 14 shows that, in Stratus I, the mixing fraction f is ~0.03 throughout the simulation. Radiation contributes ~ −0.35 K, evaporation contributes ~ +0.05 K, and entrainment mixing contributes ~ +0.15 K, to the updraft–downdraft buoyancy difference. (The sudden jump in all these fields between the 37th and 38th recorded fields is due to a jump of the cloud-top height to the next grid level.) A positive ΔT_{mix} means that entrainment mixing incorporates more warm air into downdrafts than updrafts, which is expected as discussed in Moeng et al. (1992). However, it seems strange that ΔT_{evp} is also positive, although it is very small. Note that ΔT_{evp} defined in (3.16) includes not only evaporative cooling due to entrainment mixing but also condensation warming as a result of the cloudy air being directly cooled by radiation. [This is due to the fact that we use the same ΔT_{rad} to modify h_l and s_v. Since $h_l \equiv s_v - Lq_l$, the change of saturation mixing ratio (and hence q_l) due to radiative cooling is included in ΔT_{evp}.] In Stratus I, evaporative cooling due to entrainment mixing is smaller than condensation warming resulting from radiation. However, this is not the case when, instead, evaporation from entrainment mixing dominates in determining ΔT_{evp}, as in Stratus II and III, where ΔT_{evp} is clearly negative. In any case, Fig. 14 clearly shows that, in Stratus I, cloud-top radiative cooling is the only mechanism driving turbulent circulations.

Figure 15 shows that in Stratus II f decreases from ~0.1 to ~0.02, indicating that the updraft–downdraft moisture difference decreases, according to (3.12). Both radiation and evaporation contributed about the same (from ~ −0.3 K to ~ −0.1 K) to the updraft–downdraft buoyancy difference at these near-cloud-top levels. The mixing process (without evaporation) contributes ~ +0.5 K at the earlier stage and ~ +0.1 K toward the end of the simulation.

In Stratus III (Fig. 16), the magnitude of ΔT_{evp} is nearly twice as large as that of ΔT_{rad}. So, evaporative cooling is clearly the dominant factor in making downdrafts negatively buoyant, and thus, it is the dominant process in driving boundary-layer circulations throughout the simulation.

4. Controlled experiments: NO-EVP and NO-RAD

Based on our discussion in the introduction, we expect that the positive feedback mechanism between entrainment and boundary-layer circulations exists in Stratus III and led to cloud breakup. A straightforward way to confirm this is to correlate the time evolution of the entrainment rate and circulation strength (or the layer-averaged TKE). During the cloud breakup in Stratus III, however, both radiative and evaporative cooling, the two main driving sources for turbulence, decreased drastically. Accordingly, the circulation strength (or the TKE as shown in Fig. 6c) decreased. Therefore, it is difficult to measure the positive feedback by looking at the time evolution of entrainment rate and turbulence strength. Instead, we showed in section 3c that the key process in the positive feedback loop (i.e., cloud-top evaporative cooling) is indeed the predominant driving force for boundary-layer circulations in Stratus III.

To further test this hypothesis, we discuss a controlled experiment that excludes the cloud-top evaporative cooling to see if the cloud layer would still break up without it. To turn off the latent heating/cooling, we simply set the thermodynamic variable s_v equal to h_l in the LES code. Thus, in this dust cloud (or dry cloud) simulation "liquid water" can still be "condensed" from or "evaporated" to water vapor, but *no* latent heating or cooling occurs. This controlled experiment, NO-EVP, is designed as follows: *After* the imposed 9 K/150 s free-atmospheric cooling at the 11 250th time step, we turned off latent heat effects. This way, cloud-top evaporative cooling due to entrainment mixing is excluded, while other processes remain the same as in Stratus III. We did not have to run NO-EVP for long to see the difference. Figure 17 shows its cloud-top height, cloud amount, layer-averaged TKE, and maximum horizontally averaged longwave radiative cooling. Without the evaporative cooling, the stratus deck maintained a cloud cover of 92%–98%, from the 11 250th to 14 250th time step. We also plot the jump conditions of R, the actual minimum buoyancy just below cloud top, and D_1 in Fig. 18. Compared with Fig. 9, the R and D_1 values of NO-EVP are surprisingly similar to those of Stratus III, although this cloud deck remains nearly solid. Without evaporation, $\Delta_1 = \Delta_2 > 0$, and thus, χ^* is infinity. Because the artificially enhanced entrainment due to our imposed cooling is the same as in Stratus III, this experiment clearly shows that the imposed cooling alone did not lead to breakup.

We next performed another controlled experiment that switched off radiation effects, instead of evapora-

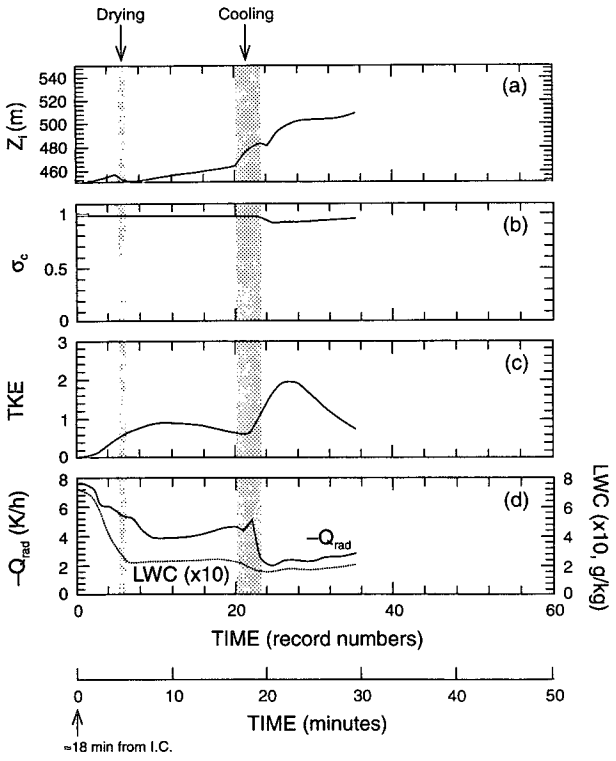

FIG. 17. Same as Fig. 6 but for the NO-EVP case.

tion effects. Like NO-EVP, this NO-RAD experiment starts from the 11 250th time step of Stratus III flow, that is, again *after* the 9 K 150 s^{-1} imposed cooling, but with the longwave radiation turned off instead. Thus, turbulent circulations with NO-RAD are driven solely by cloud-top evaporative cooling. Again, we did not have to run this case for long to see the difference. Figure 19 shows that the NO-RAD cloud dissipates as fast as Stratus III. All resultant jump conditions (not shown) are the same as Stratus III. This confirms the hypothesis that circulations in a cloud-topped PBL must be driven predominantly by cloud-top evaporative cooling, rather than radiative cooling, for the clouds to dissipate. From this study, however, we are unable to derive a threshold, indicating the relative dominance of evaporative cooling, for cloud breakup.

5. Discussion and conclusions

Observational evidence exists that a solid cloud deck may persist even when its jump condition satisfies the LRD criterion. In this study, we took another look for cloud breakup, taking into account the competition between entrainment–radiation and entrainment–evaporation feedbacks. A positive feedback exists when cloud-top evaporative cooling becomes the major driving source for boundary-layer circulations: stronger entrainment enhances cloud-top evaporative cooling, which promotes stronger circulations, which in turn enhances entrainment. Under this condition, the cloud layer is likely to break up quickly. On the other hand, the feedback between radiative cooling and entrainment (without evaporation) is negative; so when the radiative feedback dominates, runaway entrainment does not occur even if the LRD criterion is satisfied and the cloud remains solid.

To prove this, we performed three large eddy simulations (LESs) of stratus-topped PBLs. We first simulated a case (Stratus I) that is stable with respect to the LRD criterion; the resultant cloud cover remains 100%. We then "transformed" (through imposed drying and cooling of the above-cloud air) the solid cloud case into an unstable regime with respect to the LRD criterion to form Stratus II; in this case, the resultant cloud cover remains at ~85%. In the third case (Stratus III), which was "transformed" a little further into the unstable regime, the cloud dissipates very rapidly. We then analyzed and compared these LES flow fields to show that cloud-top evaporative cooling is indeed the dominant source driving the boundary-layer circulations in Stratus III but not in Stratus I or II. In Stratus I radiative cooling is the sole source driving the boundary-layer circulations, while in Stratus II cloud-top radiative and evaporative cooling contribute about equally.

Due to computer limitations, we were unable to "transform" an existing cloud deck into the CTEI regime gradually. It is clear that our imposed drying and especially cooling (which cooled the free-atmospheric

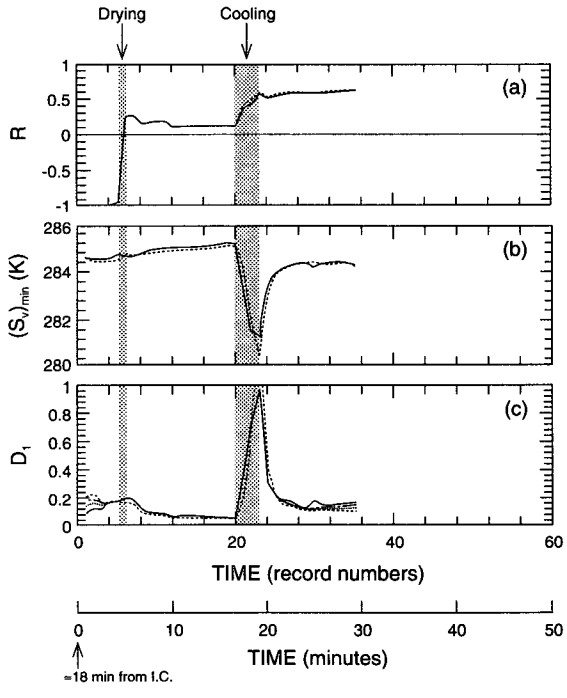

FIG. 18. Same as Fig. 9 but for the NO-EVP case.

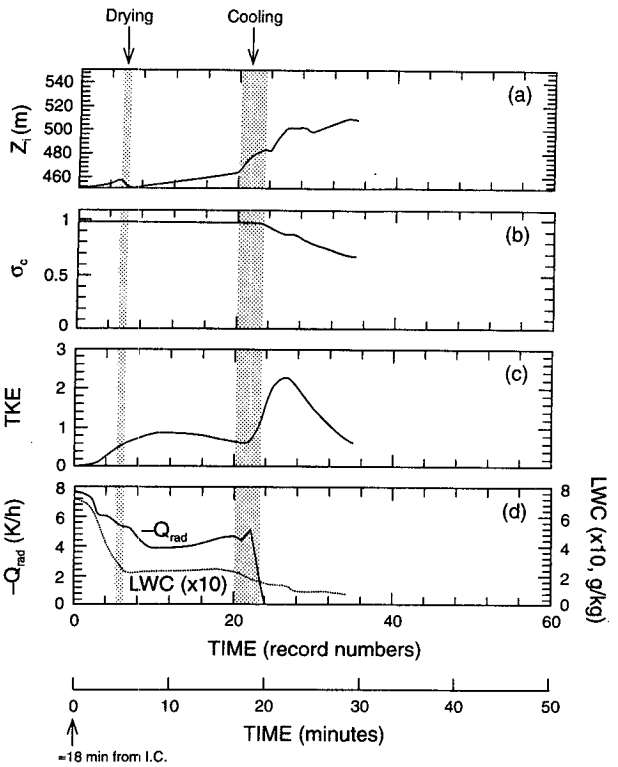

FIG. 19. Same as Fig. 6 but for the NO-RAD case.

air by 9 K in 150 s) are too abrupt. Ideally, the timescale of the change in the free atmosphere should be much longer than the turbulent turnover time (which is about 10 min in our cases), so the PBL turbulence has enough time to adjust to the "external" changes and to reach some quasi-steady state. However, current computer resources are insufficient for such a gradual change.

To confirm that our procedure of abruptly "transforming" a cloud layer into the unstable regime was not the main reason for the cloud breakup in Stratus III, we also performed two controlled experiments, NO-EVP and NO-RAD. These experiments were identical to Stratus III except that evaporative cooling was excluded in NO-EVP and radiative cooling was excluded in NO-RAD, *after* the cloud was "transformed" into the CTEI regime. Thus, the positive feedback mechanism mentioned above cannot occur in NO-EVP. The resultant cloud layer in NO-EVP remains solid, with a cloud cover of ~97%. In the NO-RAD case, where cloud-top evaporative cooling was the sole driving source for the circulations, the cloud deck dissipates as fast as Stratus III. These controlled experiments thus demonstrate the important role of the evaporative feedback on the cloud breakup process.

Of course, other physical processes that are not taken into account in our study (such as surface heat flux, shear, internal solar heating, and drizzle effects) are also likely to modify the effect of CTEI on cloud breakup, as pointed out by, for example, Turton and Nicholls (1987) and Wang and Albrecht (1994), and should be investigated in the future. Furthermore, this study assumes that the mixing process to commingle the mixture within each grid box occurs instantaneously at each time interval, which is only 0.2 s. In nature, a complete mixing within a 12.5-m cube volume may take a longer time.

It would also be interesting to compare results here with observations. Conceptually, the technique of estimating the relative contributions of radiative and evaporative cooling and entrainment warming (without evaporation) could be applied to aircraft measurements on a flight leg just below cloud top. The mixing fraction f in (3.12) could probably best be obtained by using a conserved tracer such as ozone (e.g., Wang and Albrecht 1994), instead of total water to avoid error due to drizzle. The averaged liquid water static energy (or liquid water potential temperature) and virtual dry static energy (or virtual potential temperature) within all updrafts and all downdrafts, respectively, required in solving (3.15), (3.17), and (3.19) can be obtained from conditional sampling. For this comparison study, we plan to use the Atlantic Stratocumulus Transition Experiment data.

Acknowledgments. We would like to thank Doug Lilly, Ilga Paluch, and Steve Siems for their helpful comments. CHM was partially supported by SDSM&T Contract No. IAS-NCAR-91-1 under ONR Grant N00014-91-J-4017. DAR was supported by NASA Grant NAG-1-893 to Colorado State University.

REFERENCES

Albrecht, B. A., 1991: Fractional cloudiness and cloud-top entrainment instability. *J. Atmos. Sci.*, **48,** 1519–1525.

——, R. S. Penc, and W. H. Schubert, 1985: An observational study of cloud-topped mixed layers. *J. Atmos. Sci.*, **42,** 800–822.

Betts, A. K., 1973: Non-precipitating cumulus convection and its parameterization. *Quart. J. Roy. Meteor. Soc.*, **99,** 178–196.

Boers, R., 1991: Saturation point representation of cloud-top entrainment instability. *J. Atmos. Sci.*, **48,** 2426–2435.

Breidenthal, R. E., and M. B. Baker, 1985: Convection and entrainment across stratified interfaces. *J. Geophys. Res.*, **90,** 13 055–13 062.

Caughey, S. J., and M. Kitchen, 1984: Simultaneous measurements of the turbulent and microphysical structure of nocturnal stratocumulus cloud. *Quart. J. Roy. Meteor. Soc.*, **110,** 13–34.

Deardorff, J. W., 1980a: Stratocumulus-capped mixed layers derived from a three-dimensional model. *Bound.-Layer Meteor.*, **18,** 495–527.

——, 1980b: Cloud-top entrainment instability. *J. Atmos. Sci.*, **37,** 131–147.

Hanson, H. P., 1984: On mixed-layer modeling of the stratocumulus-topped marine boundary layer. *J. Atmos. Sci.*, **41,** 1226–1234.

Krueger, S. K., 1993: Linear eddy modeling of entrainment and mixing in stratus clouds. *J. Atmos. Soc.*, **50,** 3078–3090.

Kuo, H., and W. H. Schubert, 1988: Stability of cloud-topped boundary layers. *Quart. J. Roy. Meteor. Soc.*, **114,** 887–917.

Lilly, D. K., 1968: Models of cloud-topped mixed layers under a strong inversion. *Quart. J. Roy. Meteor. Soc.*, **94,** 292–309.

MacVean, M. K., 1993: A numerical investigation of the criterion for cloud-top entrainment instability. *J. Atmos. Sci.*, **50,** 2481–2495.

——, and P. J. Mason, 1990: Cloud-top entrainment instability through small-scale mixing and its parameterization in numerical models. *J. Atmos. Sci.*, **47,** 1012–1030.

Mahrt, L., and J. Paumier, 1982: Cloud-top entrainment instability observed in AMTEX. *J. Atmos. Sci.*, **39,** 622–634.

Moeng, C.-H., 1986: Large-eddy simulation of a stratus-topped boundary layer. Part I: Structure and budgets. *J. Atmos. Sci.*, **43,** 2886–2900.

——, and U. Schumann, 1991: Composite structure of plumes in stratus-topped boundary layer. *J. Atmos. Sci.*, **48,** 2280–2291.

——, S. Shen, and D. A. Randall, 1992: Physical processes within the nocturnal stratus-topped boundary layer. *J. Atmos. Sci.*, **49,** 2384–2401.

Nicholls, S., 1989: The structure of radiatively driven convection in stratocumulus. *Quart. J. Roy. Meteor. Soc.*, **115,** 487–511.

——, and D. J. Turton, 1986: An observational study of the structure of stratiform cloud sheets: Part II. Entrainment. *Quart. J. Roy. Meteor. Soc.*, **112,** 461–480.

Randall, D. A., 1980: Conditional instability of the first kind upside-down. *J. Atmos. Sci.*, **37,** 125–130.

——, Q. Shao, and C.-H. Moeng, 1992: A second-order bulk boundary-layer model. *J. Atmos. Sci.*, **49,** 1903–1923.

Schumann, U., and C.-H. Moeng, 1991: Plume fluxes in clear and cloudy convective boundary layers. *J. Atmos. Sci.*, **48,** 1746–1757.

Shao, Q., 1994: The effects of cloud-top processes on convection in the cloud-topped boundary layer. Ph.D. dissertation, Colorado State University, 270 pp.

Shen, S., and C.-H. Moeng, 1993: Comparison of a computer-simulated stratus-topped boundary layer with aircraft observations. *Bound.-Layer Meteor.*, **65,** 29–53.

Shy, S. S., and R. E. Breidenthal, 1990: Laboratory experiments on the cloud-top entrainment instability. *J. Fluid Mech.*, **214,** 1–15.

Siems, S. T., and C. S. Bretherton, 1992: A numerical investigation of cloud-top entrainment instability and related experiments. *Quart. J. Roy. Meteor. Soc.*, **118,** 787–818.

——, ——, M. B. Baker, S. S. Shy, and R. E. Breidenthal, 1990: Buoyancy reversal and cloud-top entrainment instability. *Quart. J. Roy. Meteor. Soc.*, **116,** 705–739.

——, D. H. Lenschow, and C. S. Bretherton, 1993: A numerical study of the interaction between stratocumulus and the air overlying it. *J. Atmos. Sci.*, **50,** 3663–3676.

Sykes, R. I., and D. S. Henn, 1988: On the numerical computation of two-dimensional convective flow. *J. Atmos. Sci.*, **45,** 1961–1964.

Tag, P. M., and S. W. Payne, 1987: An examination of the breakup of marine stratocumulus: A three-dimensional numerical investigation. *J. Atmos. Sci.*, **44,** 208–233.

Turton, J. D., and S. Nicholls, 1987: A study of the diurnal variation of stratocumulus using a multiple mixed layer model. *Quart. J. Roy. Meteor. Soc.*, **113,** 969–1009.

Wang, Q., and B. A. Albrecht, 1994: Observations of cloud-top entrainment in marine stratocumulus clouds. *J. Atmos. Sci.*, **51,** 1530–1547.